Published in final edited form as:
Acad Radiol. 2008 August ; 15(8): 966–977. doi:10.1016/j.acra.2008.01.029.

Multi-parametric tissue characterization of brain neoplasms and their recurrence using pattern classification of MR images

Ragini Verma, **Evangelia I. Zacharaki**, **Yangming Ou**, **Hongmin Cai**, **Sanjeev Chawla**, **Seung-Koo Lee**, **Elias R. Melhem**, **Ronald Wolf**, and **Christos Davatzikos**

Abstract

Rationale and Objectives: Treatment of brain neoplasms can greatly benefit from better delineation of bulk neoplasm boundary and the extent and degree of more subtle neoplastic infiltration. MRI is the primary imaging modality for evaluation before and after therapy, typically combining conventional sequences with more advanced techniques like perfusion-weighted imaging and diffusion tensor imaging (DTI). The purpose of this study is to quantify the multi-parametric imaging profile of neoplasms by integrating structural MRI and DTI via statistical image analysis methods, in order to potentially capture complex and subtle tissue characteristics that are not obvious from any individual image or parameter.

Materials and Methods: Five structural MR sequences, namely, B0, Diffusion Weighted Images, FLAIR, T1-weighted, and gadolinium-enhanced T1-weighted, and two scalar maps computed from DTI, i.e., fractional anisotropy and apparent diffusion coefficient, are used to create an intensity-based tissue profile. This is incorporated into a non-linear pattern classification technique to create a multi-parametric probabilistic tissue characterization, which is applied to data from 14 patients with newly diagnosed primary high grade neoplasms who have not received any therapy prior to imaging.

Results: Preliminary results demonstrate that this multi-parametric tissue characterization helps to better differentiate between neoplasm, edema and healthy tissue, and to identify tissue that is likely progress to neoplasm in the future. This has been validated on expert assessed tissue.

Conclusion: This approach has potential applications in treatment, aiding computer-assisted surgery by determining the spatial distributions of healthy and neoplastic tissue, as well as in identifying tissue that is relatively more prone to tumor recurrence.

Keywords

brain neoplasm; recurrence; pattern classification; magnetic resonance imaging (MRI); multi-parametric MRI; Diffusion Tensor Imaging; computer aided diagnosis; tumor segmentation

1. Introduction

Treatment of brain neoplasms varies with their type, grade, location and extent, and often includes a combination of surgical resection, and chemo-radiation. This can greatly benefit from better delineation of bulk neoplasm boundary, as well as knowledge of the extent and degree of neoplastic infiltration. The true boundary of many neoplasms is difficult to identify

with conventional approaches, especially in gliomas which are diffuse and infiltrative. Relatively advanced imaging strategies, such as perfusion weighted imaging (PWI), MR spectroscopy (MRS) and diffusion tensor imaging (DTI), have improved evaluation in this regard, but remain limited. Tissue characterization is difficult because neoplasms are often heterogeneous, where different histopathologic grades can be present throughout an individual neoplasm. Since the margin for error is relatively small in the brain, depending on location, large portions of brain neoplasms may remain untreated or sub-optimally treated such that time to recurrence shortens and prognosis worsens.

Clinical decisions regarding glioma treatments rely, in part, on MRI before and after surgery as well as follow-up during and after chemo-radiation. Routine MRI sequences such as Fluid Attenuated Inversion Recovery (FLAIR) and contrast enhanced T1-weighted MR images are used to obtain estimates of enhancing and non-enhancing tissue, as well as of edema and/or gliosis. However this process is time and labor intensive, susceptible to inter-rater variability, and often inaccurate, especially in the setting of treatment related necrosis (TRN) versus recurrence/progression. Clinical decision making has been aided by the efforts of the medical image analysis community in developing MRI-based automated tumor detection and segmentation [1-9].

A simplified view of a brain neoplasm includes enhancing neoplasm/tumor (ET) tissue and non-enhancing tissue (NET) (solid tissue), and edema (diffuse tissue). As the manifestation of each of these tissue types varies across subjects and has different underlying pathological substrates depending on the neoplasm type, there has been growing interest in image-based objective identification of these tissue types as well as possible infiltration. For example, a combination of T1 (with and without IV contrast), T2 and PD-weighted images have been used in a fuzzy clustering framework to segment ET [6] and NET [5]. FLAIR images show infiltrating neoplasm and edema with relatively high contrast. Non-conventional imaging protocols, such as diffusion weighted imaging (DWI) and cerebral blood volume (CBV) maps calculated from PWI, have demonstrated the ability to discriminate between high and low grade neoplasms and also to study prognosis or predict outcome but are non-specific in identifying tumor boundary [10-12].

DTI [13] has been used for determining fiber tract deformation as a result of neoplasm growth [14-17], as well as to study the progression or infiltration of the neoplasm along white matter tracts [18,19]. Some studies have used anisotropy and diffusivity information provided by fractional anisotropy (FA) and apparent diffusion coefficient (ADC) maps computed from DTI data for differentiation of infiltrating neoplasm and edema [14,18-21]. DTI metrics have also shown potential in discriminating tumor recurrence from radiation-induced necrosis [22].

A few key issues are apparent with regard to the potential of multi-parametric MRI in studying brain tumors. First, while individual MR modalities provide information about some aspects of the tumor, no single modality is capable of providing a comprehensive tissue characterization. Properly combining such diverse MR protocols is likely to enhance discriminatory power and specificity, and to better highlight the extent and degree of tumor infiltration. Second, tissue characterization that reveals the degree and extent of infiltration is important for tumor characterization in addition to bulk tumor segmentation; however, little has been done to identify the likelihood of recurrence in the tissue surrounding the neoplasm, based on multi-parametric imaging. Third, most of the methods developed have not used advanced pattern classification techniques to discern the patterns of tissue types and infiltration or increase the objectivity of interpretation. .

The current work proposes a multi-parametric neoplastic tissue characterization that incorporates high dimensional intensity features created from multiple MRI acquisition

protocols (structural MRI as well as DTI) into a pattern classification framework, to obtain a voxel-wise probabilistic spatial map called a Tissue Abnormality Map that reflects the likelihood that a given voxel (spatial location) is healthy tissue, tumor, edema, neoplastic infiltration or a combination thereof. Moreover, by using machine learning methods guided by the follow-up scans, the likelihood of a region presenting tumor recurrence after treatment is determined. By evaluating patients with several different high grade brain neoplasms and using expert interpretation as a standard, it is demonstrated that such probabilistic tissue characterization is able to better differentiate between neoplastic infiltration, edema and healthy tissue than any single MR modality. More generally, it has been able to produce a subtle characterization of tumor tissue and surrounding tissue, and identify regions that later present recurrence. The accuracy of segmentation has been assessed on samples provided by experts. This study is one of the first to investigate integration of multiple MRI parameters via sophisticated nonlinear pattern classification methods to obtain a better characterization of the tumor and the surrounding tissue, as well as to investigate imaging profiles of tissue that are relatively more likely to present tumor recurrence in follow-up scans.

2. Methods

We propose a multi-parametric framework for tissue classification and production of probabilistic maps of tissue abnormality and tumor recurrence. Intensity based features computed from expert-defined training samples are integrated via a pattern classification technique into a multi-parametric imaging profile that aims at classifying brain tissue into each of the following classes: enhancing tumor (ET), non-enhancing tumor (NET), edema (ED), white matter (WM), gray matter (GM) and cerebro-spinal fluid (CSF). This multi-parametric tissue profile for neoplasms using pre-operative imaging can be extended to post-operative follow up scans to determine regions that demonstrate high likelihood of tumor recurrence.

2.1 Data Acquisition

We used two datasets, one for creating and validating the tissue abnormality map and the other for generating the recurrence map. In the former, we only have scans of one time point, and in the latter, we have longitudinal scans, across several time points, before and after surgery.

2.1.1 Creation of Tissue Abnormality Map—The population studied consisted of fifteen patients with newly diagnosed primary high grade brain tumors (eight grade 3 and seven grade 4) who had not received any therapy prior to imaging. The MR data for each patient were acquired either on a 3T Scanner (Siemens, Trio) or on a 1.5T (GE Medical Systems, Genesis Trio) scanner, under an IRB approved protocol which was HIPAA compliant; the scanner assignment was random (not related to any patient characteristics). The following sequences were acquired: T1-weighted (T1) (256×192×160, resolution .9765×.9765×1, TR:1620, TE: 3.87), T2 (512×512×19, resolution .4297×..4297×6.5, TR:4000, TE: 85), FLAIR (256×256×46, resolution .9375×.9375×3, TR:1000, TE: 147), gadolinium-enhanced T1-weighted (GAD) (256×256×46, resolution .9375×.9375×3, TR:1000, TE: 147) and Diffusion Tensor Imaging (DTI) (128×128×40, resolution:1.72×1.72×3.0, 12 gradient directions). Since studies were not always performed on the same scanner because of workflow constraints, there was some variation in TR, TE etc. However special effort was made to make the protocols highly comparable across scanners, in order to avoid introducing confounding variability in the images. For creating the multi-parametric tissue profile we used five structural MR acquisition protocols, namely, diffusion-weighted and baseline images (DWI and B0, respectively), FLAIR, T1, and, GAD and two scalar maps computed from the diffusion tensor images: FA and ADC [13]. Fig. 1 shows representative slices from each of the acquisition protocols.

2.1.2 Creation of recurrence maps—The cases chosen are representative of tumor recurrence as a result of tumor infiltration into surrounding healthy tissue or due to incomplete resection. Our framework focuses on these ambiguous regions that have a mixture of neoplastic and normal tissue characteristics with the aim of classifying them to one of these two classes of normal and neoplastic tissue. The selection of the patients followed three criteria:

(a) no evidence for residual enhancing tumor existed after the first resection (based on the clinical reports created by examining the postoperative images acquired within the same day);

(b) the patients have shown obvious recurrence confirmed by pathology and a second craniotomy; and

(c) all of the 7 MR protocols (required for the multi-parametric tissue profile discussed above) were available in the pre-resection stage; not all protocols were required in the post-resection stage. Specifically, the search in the post-resection images for regions with characteristics of recurrence was mostly based on visual evaluation of FLAIR, T2 and GAD images, and CBV maps (computed from perfusion images). The CBV maps help distinguish between radiation treatment effects and tumor recurrence. None of the images from the post-resection scans (including CBV maps) were used in the training for creating the multi-parametric profile (probabilistic map).

Of the available brain tumor cases, 3 cases met all the above criteria and have been included.

2.2 Preprocessing

The images are skull stripped and smoothed using the public software package FSL [23]. For each of the patients, all the modalities are rigidly co-registered to the T1-weighted image using FSL's registration algorithm, called FLIRT [24] (rigid registration suffices as it is within the same patient). Data is made comparable across patients using histogram matching of intensities. In order to create the feature vectors, we fuse information from the same voxel across different imaging protocols of the same person. In order to extend the profile to a recurrence map, we register the follow-up (post-resection) images to the pre-resection image using deformable registration [25], as non-linear deformations are introduced due to the relaxation of tumor mass effect. The co-registration of all temporal images is important to keep track of changes that reflect tumor progression and for mapping the region of tumor recurrence from the post- to the pre-operational space.

2.3 Design of Tissue Abnormality Feature Vector

We define voxel-wise intensity features using the aligned and pre-processed MR images. The *intensity feature vector* for each voxel $\vec{x}$ in the 3D image volume I, is defined by concatenating all 7 image values:

$$\vec{v}_{\vec{x}} = \left[I_{\vec{x}}^{(ADC)}, I_{\vec{x}}^{(B0)}, I_{\vec{x}}^{(DWI)}, I_{\vec{x}}^{(FA)}, I_{\vec{x}}^{(FLAIR)}, I_{\vec{x}}^{(T1)}, I_{\vec{x}}^{(GAD)} \right]^T$$

where $I_{\vec{x}}^{(M)}$ denotes the intensity of image of modality M at voxel $\vec{x}$. These feature vectors are defined at each voxel in the training samples. In order to render this feature vector more robust to noise, we incorporate neighborhood information by using four of its neighbors. 7 dimensional intensity features for these 5 voxels are stacked into a long vector (35 dimensional), which is then used as a feature vector.

2.3.1 Selection of the training samples—Training samples are identified by an expert neuroradiologist (co-author) by delineating small portions of the tumor tissue types of ET, NET and ED, using the FLAIR and GAD-T1 images. The training samples for ET, NET and ED are picked very conservatively (only those that have a high certainty according to the expert) as

demarcated in red in Fig. 2 (columns 1 and 2). We obtain training samples for the healthy tissue by automatically segmenting the healthy portion of the brain into three classes: WM, GM and CSF using a k-means segmentation algorithm provided by FSL, called FAST [26], excluding regions close to the tumor. By segmenting the healthy portion of the brain during training we are able to build a different model for each of the WM, GM and CSF classes, and therefore avoid the repeated application of a segmentation method, like FAST, to all new coming brain tumor images. It may be noted that the algorithm is being designed to emulate the knowledge of the expert and hence depends on the expert's definition of the regions. Using multiple experts will increase the size of training samples and is expected to lead to better classifiers. However, conflicting regions of definitions between the experts indicate areas with low certainty about the tissue type and therefore need to be removed from the definition prior to using them as training samples.

2.3.2 Creation of Tissue Classifiers and Tissue Probability Maps—We investigated several pattern classification techniques that are available in the literature that can help create tissue classifiers. We found that linear multivariate pattern classification techniques such as PCA (Principal Component Analysis) are easier to apply but they create “global” features for each class that are insufficiently representative for discriminating one tissue class from another, especially when the difference between two classes is very subtle, which will be the case in tumor components (NET and ED) and in infiltration. SVM (Support Vector Machines) [27] were found to optimally classify the data into two or more classes [28,29]. We construct two kinds of classifiers using two different non-linear classification strategies optimized for the respective application: 1) *Intra-patient classifier*: Bayesian classifiers [30] trained using expert defined training samples from within a single patient; and 2) *Inter-patient classifier*: SVM classifiers trained by combining samples from several patients. For the purposes of comparison, Bayesian classifiers are also constructed using data from several patients. Validation of the classifiers is done by creating classifiers using only part of the expert defined training samples, and then applying the classifiers to those excluded samples to determine how well the classification agrees with the expert's interpretation [27]. The amount of agreement is referred to as the classification accuracy.

Intra-patient classification: We use Bayesian classification method, to design discriminant functions [30] for each of the 6 tissue classes for a subject, that we refer to as the respective tissue class classifiers. Different discriminant functions designed for each of the 6 tissue classes, i.e. ET, NET, ED, WM, GM and CSF, evaluated at each voxel, provide the estimate of the probability of that voxel belonging to the respective class, and produce a 3D voxel-wise probability map, called Tissue Abnormality Map. There is one Tissue Abnormality Map pertaining to each of the 6 tissue classifiers produced by assuming multivariate Gaussian distribution for the features. We can obtain tissue segmentation by assigning the voxel to the class having the highest discriminant value, among the six classes. This method of tissue classification is optimal when training samples are available for the patient whose tissue needs to be characterized. It effectively replicates the experts' samples to identify regions that are similar. However, only tissue classes (ET, ED, NET) identified by the expert can be characterized for that patient, and due to the conservative nature of sample selection, may not reflect the presence of the alternate tissue types for which no expert identification was provided. This requires pooling samples from several patients and due to the high variability across individuals, Bayesian classification with its multinomial Gaussian assumption does not provide adequate classification.

Inter-patient classification: We combine training samples from across patients, to obtain a more generalized tissue classification using SVM. We define 6 classifiers, one pertaining to each of healthy (WM, GM and CSF) and neoplasm (ET, NET and ED) classes [27]. Each

classifier is created using two sets of training samples, one containing samples of the tissue type for which the classifier is being created, and the second class containing samples from all other tissue classes combined together. This is referred to the one-versus-all framework of creating a classifier and details can be found in [27]. When these classifiers are applied to features defined at voxels in a new brain, they produce a number (SVM classification score) indicative of the class membership (tissue type). This SVM score is then converted to a pseudo-probability score p_platt using Platt's method [31]. Then the probability values are normalized: p_normalized = p_platt /sum(p), where sum(p) is the sum of platt probabilities for all classes. These voxel-wise pseudo-probability scores form the Tissue Abnormality Map pertaining to that classifier. Responses from the classifiers are combined to obtain tissue segmentation, i.e. labels are assigned according to the maximum probability (after normalization). The classifiers are validated using a similar framework to the one adopted in intra-patient classification.

2.4 Design of Recurrence Map

Fig. 3 provides examples of recurrence maps for 3 cases. The top row shows slices from post-resection scans: CBV maps computed from perfusion images and T1 images (with/without contrast) that indicate regions of likelihood of recurrence characterized by increased enhancement in GAD (cases 2, 3) and high CBV (case 2) or hypointensity in T1 (case 1, 3), which are regions indicative of high risk (indicated by green arrows). Visual cues gathered from these scans were combined with the cues obtained by elastically registering the post-resection scans with the pre-resection scans (shown in bottom row, left) to account for tissue deformation caused by resection, and to guide the determination of the position of these probable recurrence regions in the pre-resection scans (marked in burgundy in bottom row). Since no evidence for residual enhancing tumor existed after the resection, these regions were likely to be on or outside the visible tumor boundary pre-resection and developed abnormality over time possibly due to tumor infiltration. Samples for the healthy class depicted in blue (Fig. 3, bottom row) were delineated close to the tumor as well as away from it, in order to sample the variability fully. These samples were used to train a two class SVM classifier. At each instance of training, one patient was left out. Then the classifiers, applied to this left-out patient, produced voxel-wise SVM scores of the tissue at that voxel demonstrating recurrence. These voxel-wise SVM scores comprise a *recurrence probability map* that is indicative of the voxel-wise likelihood of recurrence.

3. Results

The experiments were conducted with the aim of identifying the applicability of the multi-parametric framework in distinguishing between neoplastic tissue types in patients and identifying regions that have a high likelihood of recurrence. In all these experiments, our aim was to produce 3D voxel-wise spatial probability maps for each tumor tissue type, however we have also produced maps of hard segmentation in order to validate the results visually and empirically. We use classification rates and sensitivity and specificity values, computed on some of the expert defined samples excluded from training, to provide a measure of degree of certainty in identifying the tumor and the healthy tissue. Classification rate is the percentage of correctly classified voxels with respect to the total number of training voxels available for that class. Therefore, there is one value for each of the 6 class. We take the average over all the subjects for that class to produce the average values for each of the classes.

The sensitivity and specificity are calculated on the two-class problem by grouping together the tumorous tissue types ED, ET and NET into one class (positive class) and the healthy tissue types CSF, GM, WM into an other class (negative class), respectively. The sensitivity and specificity show the percentage of correctly classified positive and negative samples respectively. Sensitivity = TP*100 / (TP + FN) and Specificity = TN*100 / (FP + TN) where

TP, TN, FN, FP stand for true positive, true negative, false negative and false positive respectively.

3.1 Intra-patient Tissue Classification

Figure 2 shows the results of applying the Bayesian classification framework (section 2.3.2) on 3 of the 14 patients. Each row corresponds to a different patient and shows examples of expert-defined neoplastic regions that are used as training samples, the tissue probability maps, as well as hard tissue segmentation obtained from these probability maps. The top left corner of each probability map gives the classification accuracy for that tissue in that patient. For some patients, where the expert was unable to define certain tissue types, such as NET in rows 2 and 3 of Fig. 2, no probability maps could be created. The average classification rates over all datasets can be found in row 1 of Table 1.

3.2 Inter-patient tissue classification

The comparative results of applying the inter-patient, Bayesian and SVM, tissue classifiers can be found in Table 1, row 2 and 3, respectively. As can be observed, Bayesian classification (row 2) performed poorly in the inter-patient framework, i.e., in the case of increased variability in the data, due to the combination of training samples from several patients, as compared with the intra-patient Bayesian classification (row 1).

By combining the training samples from different patients, we can combine information from patients within a grade and apply to other patients of the same grade. Empirically, we found that keeping within the grade produces probability maps that are high in specificity. The average sensitivity and specificity for all patients can be found in the last columns of Table 1.

For visual assessment, we show the application of the inter-patient tissue classifiers on a case with non-enhancing tumor (Fig. 4) and on a case with enhancing tumor (Fig. 5). The first column in both figures provides slices from the FLAIR and GAD image to indicate the extent and composition of the tumor. The top row 1 (column 2 – 4 for Fig. 4 and column 3 – 6 for Fig. 5) shows the probability maps and tissue segmentation map obtained by applying the SVM classifiers (section 2.3.2) to this patient and the bottom row the Bayesian classifier (created using training samples from all patients except this patient). The comparative classification rates and sensitivity and specificity for these patients are given in Table 2. In Fig. 4, there was no ET detected in the tumor, the NET was over-segmented by the Bayesian framework (as is also evident from the tissue probability maps for NET which shows high false positives). The entire tumor was classified as NET failing to detect the tissue differences. The SVM framework was able to characterize the tumor as a combination of edema and NET and the dark core was classified as CSF, perhaps due to the nature of the tissue. In Fig. 5, we see the example of a case in which the Bayesian framework provides better segmentation, which is also reflected in the classification accuracy in Table 2. However SVM performs better in determining healthy tissue with low false positives.

3.2 Analyzing Patterns of Tumor Recurrence

As explained in section 2.4, recurrence classifier created from two patients was then applied to the features computed from the pre-resection scans of the third patient, to create a recurrence probability map, indicative of regions with high likelihood of recurrence. Fig. 3, bottom row, right, shows the recurrence probability maps for three cases. Although these results are preliminary and the number of patients is very small to be able to draw a conclusion, it can be observed that regions that were identified as recurrence in these patients, actually showed high probability (red) of abnormality in the pre-resection scans.

4. Discussion

In this study we have created a multi-parametric profile for brain tumors, aiming at a comprehensive tissue characterization. Both classification approaches (intra- and inter-patient with Bayesian and SVM classification) have the same underlying framework, namely combining conventional structural MRI with DTI, to train classifiers for the tumor types of enhancing and non-enhancing tumor, edema and healthy tissue. The distinction of the neoplastic tissue from healthy tissue, as well as the identification of different tumor components and edema, as can be seen in Figs. 4-5, indicates that this multi-parametric framework effectively integrates multi-protocol information into a comprehensive tissue profile that can systematically evaluate the extent and heterogeneous composition of the tumor, and accurately replicate the expert's outlining of these regions. Thus, knowing the probable extent of abnormality of the neoplasm in terms of enhancing or non-enhancing tumor type or edema, will help better target the treatment of these regions. Existing computerized methods for diagnosis suffer from the absence of validation due to the lack of ground truth. Conventionally, histopathological exam following a biopsy has been the accepted ground truth. However its outcome depends on the region sampled and given the heterogeneity of the tumor, may wrongly indicate the grade of the tumor and the subsequent treatment. The probability measures of our framework are defined on each voxel, and therefore capture heterogeneous patterns of tissue pathology. Moreover, these maps may provide sufficient premise to histologically test regions with higher probability of neoplastic content. This would aid in making clinical decisions.

Indeed, tissue that shows mixture of healthy and neoplastic tissue, with or without edema, may be a precursor to the development of a neoplasm in the future. This is precisely the aim of the experiments that we have conducted on cases that have demonstrated recurrence (Fig. 3). By identifying regions in the pre-resection scan that correspond to the recurring neoplasms in the follow-up scans, we have characterized the imaging profile of abnormal tissue that transformed to a neoplasm. Although we have used a small dataset for the identification of regions of high abnormality and high tumor recurrence probability, the quantification of the degree of abnormality by the probability maps in this manner illustrates the concept of anticipating sites of recurrence requiring more aggressive or alternate therapies. Thus, although we might not always have accurately determined the regions of recurrence, we have been able to demonstrate that the regions we predicted to recur, based on the probabilistic maps produced by the classification framework, did actually progress to recurrence.

We have proposed intra- and inter- patient approaches to the characterization of neoplastic tissue, based on very conservative training samples identified by experts. The approach that is to be finally adopted depends on the application. If the aim is to replicate the understanding of the expert for a particular patient, as may be the case in a surgery-related decision, then the intra-patient Bayesian framework is the best (as can be seen in the classification rates and the good segmentation maps in Fig. 2). While useful for individual patient analysis, such a profile can only be applied to future scans of that patient alone, owing to the fact that the profile will not be able to capture the variability across patients. An analysis of the probability and the segmentation maps reveals that the framework tends to over-segment tissue types (such as ET in patient of row 1 and edema in patient of row 2, in Fig.2). Additionally, the intra-patient Bayesian framework is unsuitable for determining a tissue type that the expert is unable to identify, or even do the characterization of the patient for which no training samples are available. This is especially the case when there is a large mass of NET and edema which is difficult to distinguish even by the expert. When treatment decisions need to be made about surrounding non-enhancing tissue, it is important to have a tissue characterization that will highlight the regions of abnormality. This was the motivation to develop the inter-patient framework.

The evaluation of the SVM and Bayesian classification methods in combining tissue samples across patients, indicates SVM performs better. A comparison of row 2 and 3 of Table 1 shows that the Bayesian classifier has lower sensitivity than the SVM, and also demonstrates increased classification accuracy (with lower variability) for the SVM classifier in all tissue types except NET. Edema identification shows marked improvement. ET is also identified with high classification accuracy based on the expert defined samples. The comparison reveals that NET was the most difficult tissue type to characterize both by the computerized algorithm as well as the experts, demonstrated by the fact that the expert identified the least training samples for NET. This is indicative of the variability in these regions across patients. There is a decrease in the average classification rate of NET from the inter-patient Bayesian to the SVM classification, although both are low, which could be due to the low number of training samples to which SVM is sensitive. Based on the improved performance in the other tissue classes, we expect SVM to do better when we add training samples in the future. While it may seem that the intra-patient Bayesian classification performs very well in the case of NET, it should be noted that this is only true for patients in whom NET has already been identified by an expert and the average classification rates have been computed only on these few subjects. Analysis of the NET classification results with inter-patient classification reveals that it is mostly mis-classified as edema, GM and CSF or a possible combination of these. This could be explained by the fact that NET could have healthy tissue combined with neoplasm and edema and NET could be easily mis-classified by an expert too. The superiority of inter-patient classification reveals that a combination of information from several patients is crucial for generalizability when a new patient is to be tested in this framework. We propose to use additional features and better SVM based classifiers to pursue inter-patient classification of tumor types.

Conclusions

In summary, we have tested a multi-parametric framework for neoplastic tissue characterization using multiple MR acquisition protocols. This abnormality profile helps distinguishing between neoplastic components, edema and normal tissue, and creating a probabilistic map that indicates the likelihood of tumor recurrence. We expect that our tissue classification will be able to 1) provide a better understanding of the spatial distribution of cancer, thereby assisting in treatment planning either via resection or focused radiotherapy and radiosurgery; 2) potentially enhance the physician's ability to diagnose and segment the tumor and 3) help identifying tissue that can convert to tumor in follow up cases post resection. The method can thus potentially be used to study tissue changes introduced as a result of radiotherapy, chemotherapy and medication. Future studies are necessary to provide a more extensive training basis for the classifiers, and to further validate the performance of this computer analysis methodology. We also propose to use feature selection schemes to determine the contribution of each of the modalities, so that the modalities best for tissue characterization can be identified and the acquisition protocol streamlined.

References

1. Prastawa M, Bullitt E, Ho S, Gerig G. A brain tumor segmentation framework based on outlier detection. Medical Image Analysis 2004;8(3):275–283. [PubMed: 15450222]
2. Schmidt, M.; Levner, I.; Greiner, R.; Murtha, A.; Bistritz, A. Segmenting Brain Tumors using Alignment-Based Features; The Fourth International Conference on Machine Learning and Applications; Los Angeles, CA. 2005; Dec. 2005
3. Kaus MR, Warfield SK, Nabavi A, Black P, Jolesz FA, Kikinis R. Automated Segmentation of MR Images of Brain Tumors. Radiology 2001;218(2):586–591. [PubMed: 11161183]
4. Just M, Thelen M. Tissue Characterization with T1, T2 and Proton Density Values: Results in 160 Patients with Brain Tumors. Radiology 1988;169:779–785. [PubMed: 3187000]

5. Fletcher-Heath LM, Hall LO, Goldgof DB, Murtagh FR. Automatic segmentation of non-enhancing brain tumors in magnetic resonance images. Artificial Intelligence in Medicine 2001;21:43–63. [PubMed: 11154873]
6. Clark M, Hall L, Goldgof D, Velthuizen R, Murtagh F, Silbiger M. Automatic tumor segmentation using knowledge-based techniques. IEEE Transactions on Medical Imaging 1998;17(2):187–201. [PubMed: 9688151]
7. Young RJ, Knopp EA. Brain MRI: Tumor Evaluation. Journal of Magnetic Resonance Imaging 2006;24(4):709–724. [PubMed: 16958058]
8. Bordignon KC, Neto MC, Ramina R, de Meneses MS, Zazula AD, de Almeida LGMP. Patterns of neuroaxis dissemination of gliomas: suggestion of a classification based on magnetic resonance imaging findings. Surgical Neurology 2006;65:472–477. [PubMed: 16630907]
9. Talos I-F, Zou KH, Ohno-Machado L, et al. Supratentorial low grade glioma resectability: statistical predictiv analysis basedon anatomic MR features and tumor characteristics. Radiology 2006;239(2): 506–513. [PubMed: 16641355]
10. Aronen HJ, Gazit IE, Louis DN, et al. Cerebral Blood Volume Maps of Gliomas: Comparison with tumor grade and histological findings. Radiology 1994;191(1):41–51. [PubMed: 8134596]
11. Krabbe K, Gideon P, Wagn P, Hansen U, Thomsen C, Madsen F. MR diffusion imaging of human intracranial tumors. Neuroradiology 1997;39:483–489. [PubMed: 9258924]
12. Provenzale JM, Mukundan S, Baroriak DP. Diffusion-weighted and Perfusion MR Imaging for Brain Tumor Characterization and Assessment of Treatment. Radiology 2006;239(3):632–649. [PubMed: 16714455]
13. Bihan DL, Mangin J-F, Poupon C, et al. Diffusion tensor imaging: concepts and applications. Journal of Magnetic Resonance Imaging 2001;13:534–546. [PubMed: 11276097]
14. Nimsky C, Ganslandt O, Hastreiter P, et al. Intraoperative Diffusion tensor MR imaging: Shifting of white matter tracts during neuro-surgical procedures - initial experience. Radiology 2005;234(1): 218–225. [PubMed: 15564394]
15. Field AS, Alexander AL. Diffusion Tensor Imaging in Cerebral Tumor Diagnosis and Therapy. Topics in Magnetic Resonance Imaging 2004;15(5):315–324. [PubMed: 15627005]
16. Stieltjes B, Schluter M, Didinger B, et al. Diffusion tensor imaging in promary brain tumors: reproducible quantitative analysis of corpus callosum infiltration and contralateral involvement using a probabilistic mixture model. Neuroimage 2006;31:531–542. [PubMed: 16478665]
17. Stadlbauer A, Nimsky C, Buslei R, et al. Diffusion tensor imaging and optimized fiber tracking in glioma patients: histopathologic evaluation of tumor-invaded white matter structures. Neuroimage. 2006
18. Tummala RP, Chu RM, Liu H, Nil T, Hall WA. Application of Diffusion Tensor Imaging to Magnetic-Resonance-Guided Brain Tumor Resection. Pediatric Neurosurgery 2003;39:39–43. [PubMed: 12784077]
19. Mori S, Fredericksen K, Zijl PCMv, et al. Brain white matter anatomy of tumor patients evaluated with diffusion tensor imaging. Annals of Neurology 2002;51(3):377–380. [PubMed: 11891834]
20. Jellison BJ, Field AS, Medow J, Lazar M, Salamat MS, Alexander AL. Diffusion Tensor Imaging of Cerebral White Matter: A Pictorial Review of Physics, Fiber Tract Anatomy, and Tumor Imaging Patterns. American Journal Of Neuroradiology March;2004 25:356–369. [PubMed: 15037456]
21. Sundgren PC, Fan X, Weybright P, et al. Differentiation of recurrent brain tumor versus radiation injury using diffusion tensor imaging in patients with new constrast-enhancing lesions. Magnetic Resonance Imaging 2006;24:1131–1142. [PubMed: 17071335]
22. Hein PA, Eskey CJ, Dunn JF, Hug EB. Diffusion-weighted imaging in the follow-up of treated high-grade gliomas: tumor recurrence versus radiation injury. AJNR Am J Neuroradiol 2004;25(2):201–9. [PubMed: 14970018]
23. Smith SM, Jenkinson M, Woolrich MW, et al. Advances in functional and structural MR image analysis and implementation as FSL. Neuroimage 2004;23(S1):208–219.
24. Jenkinson M, Smith S. A global optimisation method for robust affine registration of brain images. Medical Image Analysis 2001;5(2):143–156. [PubMed: 11516708]
25. Zacharaki, EI.; Shen, D.; Mohamed, A.; Davatzikos, C. Registration of Brain Images with Tumors: Towards the Construction of Statistical Atlases for Therapy Planning. ISBI; Arlington, VA: 2006.

26. Zhang Y, Brady M, Smith S. Segmentation of brain MR images through a hidden Markov random field model and the expectation maximization algorithm. IEEE Transactions on Medical Imaging 2001;20(1):45–57. [PubMed: 11293691]

27. Schölkopf, B.; Smola, AJ. Learning with Kernels: Support Vector Machines, Regularization, Optimization and Beyond (Adaptive Computation and Machine Learning). 1st edition. The MIT Press; Dec 15. 2001 2001

28. LaConte S, Strother S, Cherkassky V, Anderson J, Hu X. Support vector machines for temporal classification of block design fMRI data. NeuroImage 2005;26(2):317–329. [PubMed: 15907293]

29. Davatzikos C, Shen DG, Wu X, et al. Whole-brain morphometric study of schizophrenia reveals a spatially complex set of focal abnormalities. JAMA Archives of General Psychiatry 2005;62:1218–1227.

30. McLachlan, GJ. Discriminant Analysis and Statistical Pattern Recognition. Wiley-Interscience; New York: 2004. Wiley Series in Probability and Statistics

31. Platt, J. Probabilistic outputs for support vector machines and comparison to regularized likelihood methods. In: Schuurmans, D., editor. Advances in Large Margin Classifiers. MIT Press; Cambridge, MA: 2000.

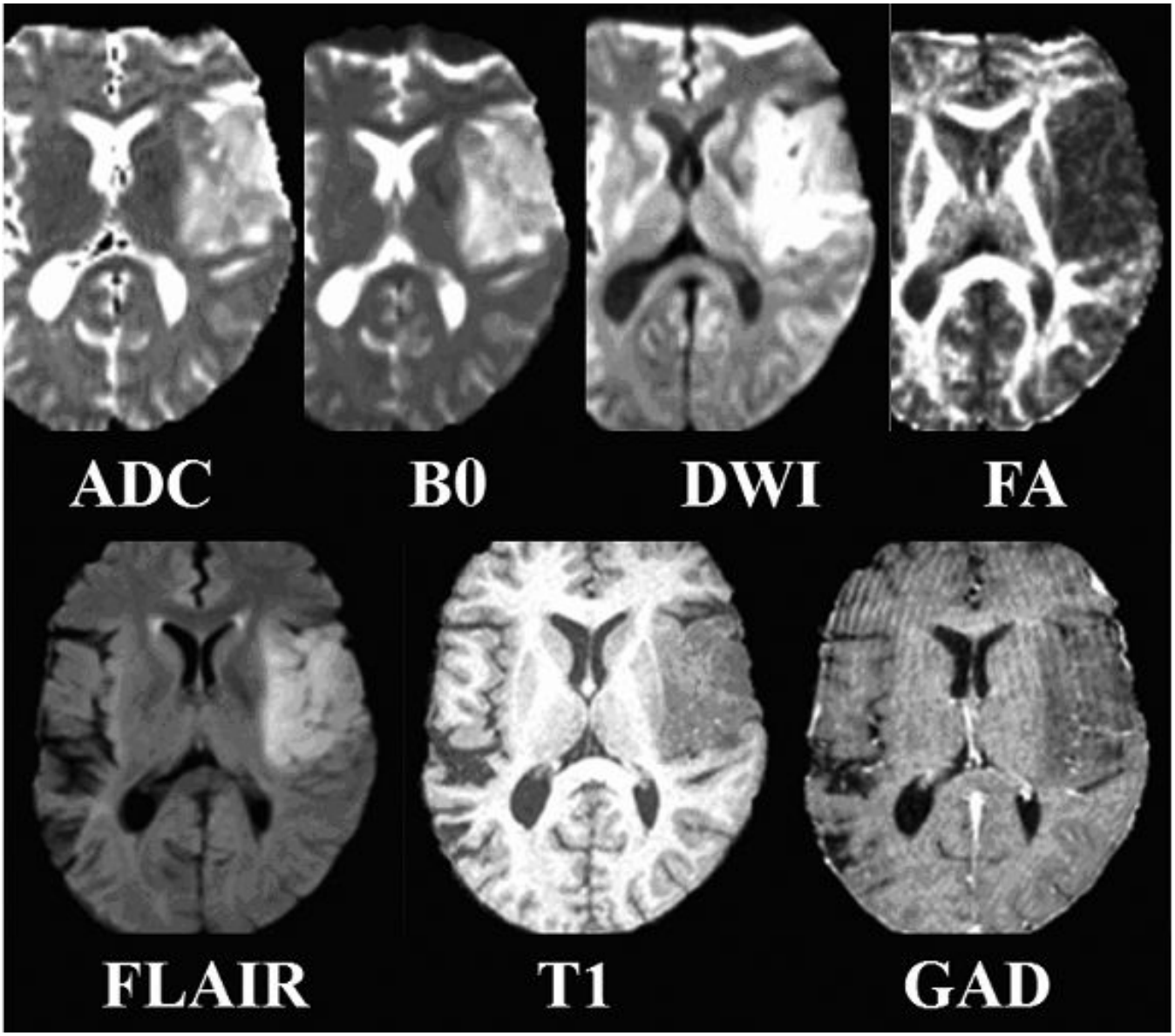

Fig. 1.
A representative slice from each of the seven co-registered MR modalities used in creating the multimodality tissue profile.

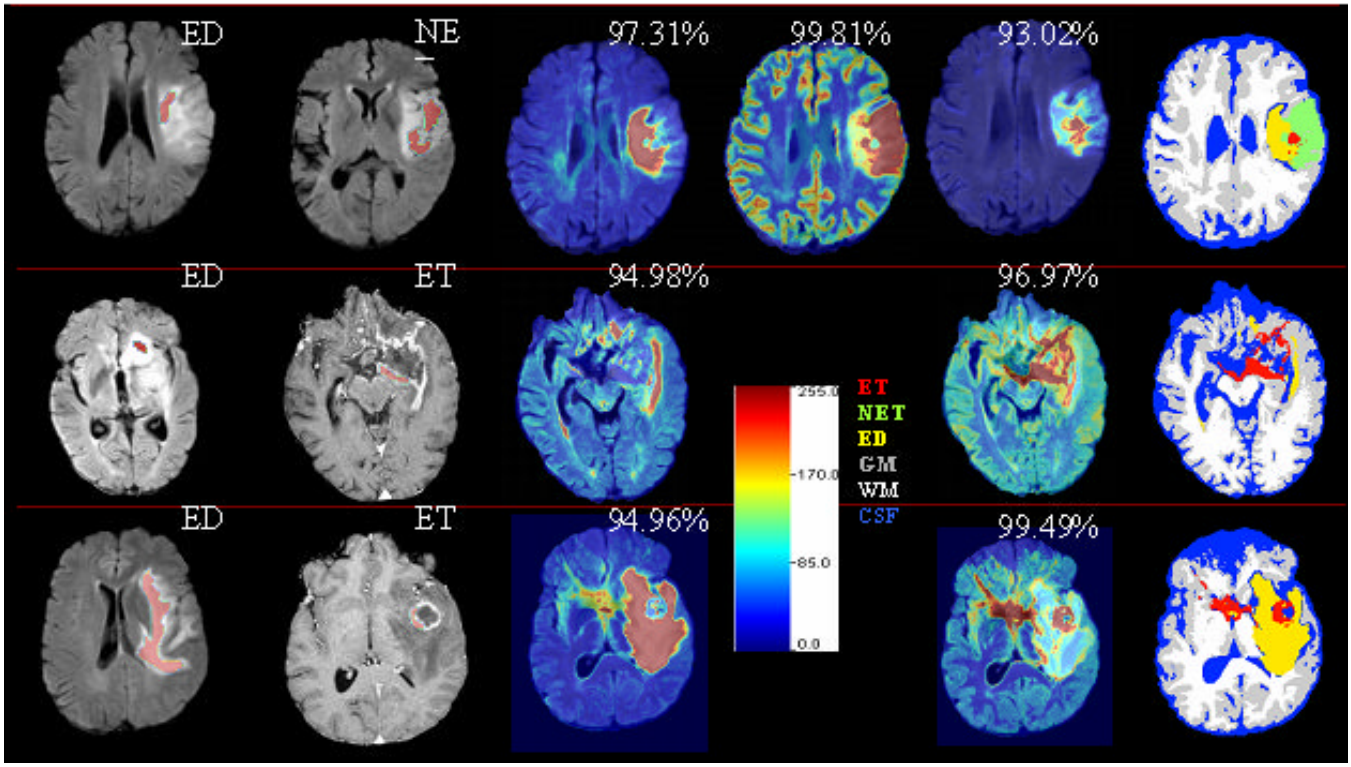

Fig. 2.

Intra-patient Bayesian classification framework applied to 3 patients. Each row corresponds to a patient. Columns 1 – 2 show examples of conservative training samples chosen by the expert for tissues samples of ED, ET and/or NET. Columns 3 – 5 are the probability maps for ED, NET and ET, respectively. The numbers in the upper left corners denote the classification rates. A missing image such as in (2, 4) block indicates the lack of training samples for that tissue class and hence the inability of the classifier to produce the corresponding probability map. The color bar for the probability maps are in block (2, 4). Column 6 shows the segmented image with the color coding of the tissues shown next to the color bar.

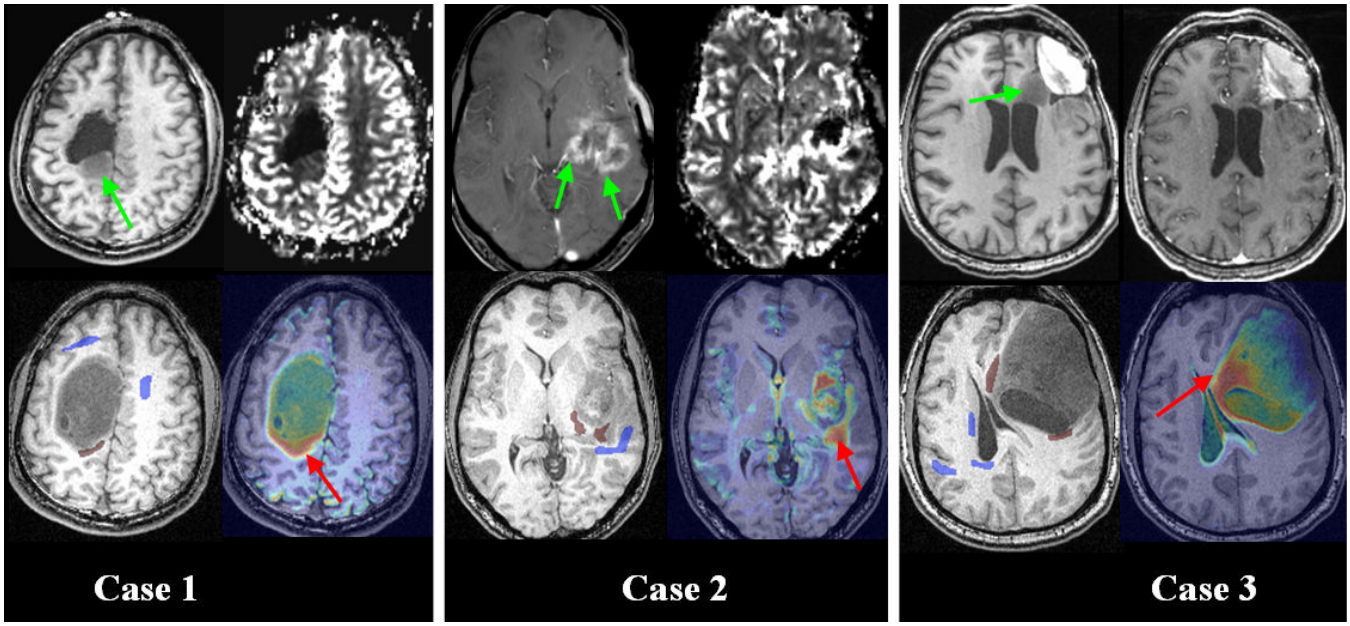

Fig. 3.

Maps of tumor recurrence for three cases. For each case, the top row shows post-resection scans; green arrows point to regions identified as suspected of possible recurrence. Bottom row, left: Pre-resection scans showing the regions used for training; blue are samples for healthy tissue; burgundy are some of the regions identified by an expert as having recurrence in post-resection scans when combined with cues obtained from elastic registration. Bottom row, right: Probability maps using inter-patient classifiers that provide a voxel-wise map of likelihood of tumor recurrence. The color bar is the same as that of Fig. 2 with red indicating higher degree of abnormality. Red arrows are used to indicate regions in which recurrence actually occurred in follow-up scans.

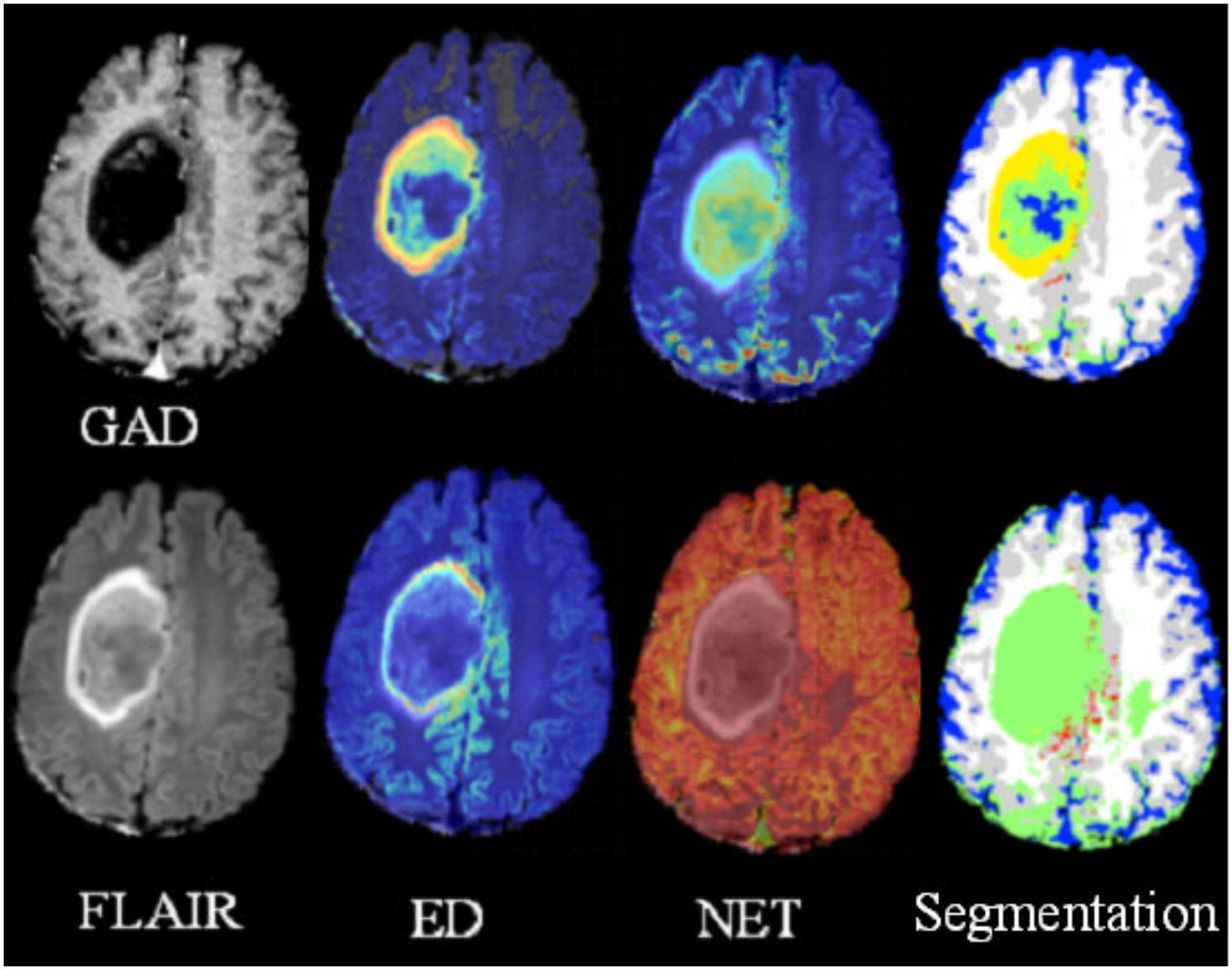

Fig. 4.

Application of SVM classification (top row) and Bayesian classification (bottom row) of the neoplasm represented in column 1 by training across patients. While SVM classifiers combining information from several patients are able to identify both ED and NET, like the expert, the Bayesian classifiers created from this patient alone identify the whole neoplastic region as NET (unlike the expert). The color-coding is same as that of Fig. 2.

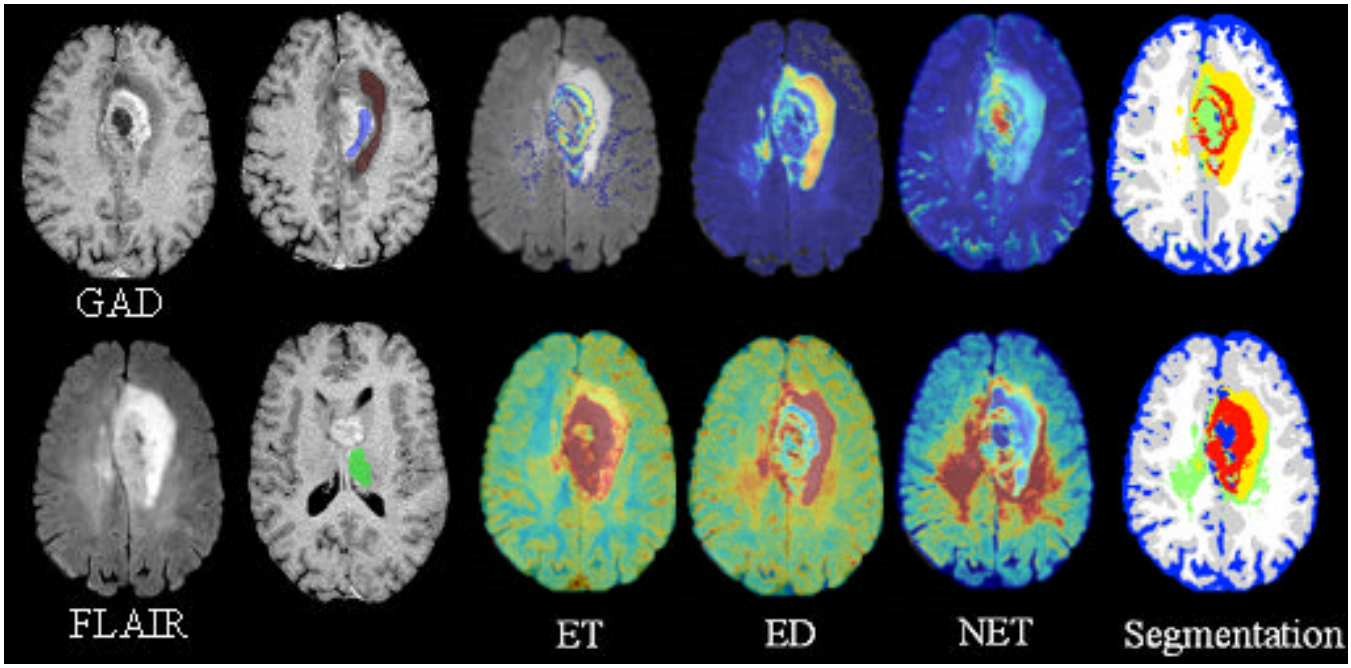

Fig. 5.

Application of SVM classification (top row) and Bayesian classification (bottom row) of the neoplasm represented in column 1 by training across patients using training samples shown in column 2. The SVM classification (top row, column 3–6) is more conservative than the Bayesian classification (bottom row, column 3–6) and matches the expert better. The probability maps using the Bayesian classification seem to identify the edema well, over-segment the ET and confuse the NET with CSF. The SVM classification is able to capture the presence of NET (green) in the segmented image on top row, along with ED and ET. The color-coding is same as that of Fig. 2.

Table 1

Average (*avg*) classification rates and their standard deviation (*stdev*) of the classification rates, sensitivity and specificity, over all subjects for intra- and inter-patient framework using Bayesian and SVM classification.

		Classification rates						Sensitivity tumor vs healthy	Specificity tumor vs healthy
		ED	**ET**	**NET**	**CSF**	**GM**	**WM**		
Bayesian Classification (intra-patient)	*avg*	97.03	96.39	93.05	89.68	74.86	82.95	91.84	99.57
	stdev	3.18	3.4	11.82	21.72	6.95	7.73	6.01	0.63
Bayesian Classification (inter-patient)	*avg*	53.86	86.56	51.11	82.31	66.78	76.06	75.62	94.57
	stdev	47.59	27.74	43.86	15.82	9.22	15.05	36.14	6.12
SVM Classification (inter-patient)	*avg*	93.38	88.79	34.01	91.34	72.21	85.33	87.54	97.03
	stdev	8.75	29.03	38.71	7.9	12.08	9.45	15.58	3.26

Table 2

Classification rates sensitivity and specificity of applying the SVM and Bayesian inter-patient classification framework to the 2 patients shown in Figs. 4 - 5. Overall, the SVM classification performs better than the Bayesian. The low classification rates of healthy tissue are due to these samples being selected through an automated segmentation method, which may have led to errors in training.

Patient in Fig		Classification rates						Sensitivity tumor vs healthy	Specificity tumor vs healthy
		ED	ET	NET	CSF	GM	WM		
Fig. 4	SVM	79.78	*NA*	56.61	78.11	81.99	84.36	71.07	99.49
	Bayes	2.28	NA	100	37.01	56.25	60.58	99.98	77.6
Fig. 5	SVM	100	11.56	NA	99.9	54.66	96.16	81.59	99.97
	Bayes	100	99.03	NA	97.87	72.84	61.26	99.02	98.11